ACS APPLIED ENERGY MATERIALS

www.acsaem.org Letter

Understanding and Advancing Bifacial Thin Film Solar Cells

Adam B. Phillips,* Kamala Khanal Subedi, Geethika K. Liyanage, Fadhil K. Alfadhili, Randy J. Ellingson, and Michael J. Heben

Cite This: *ACS Appl. Energy Mater.* 2020, 3, 6072−6078 Read Online

ACCESS | Metrics & More | Article Recommendations | Supporting Information

ABSTRACT: Because bifacial solar cells increase the power generated per area, their market share is projected to increase over the next decade. While silicon technologies have implemented bifacial technology, little progress has occurred in bifacial thin film (BTF) solar cells. Understanding the factors that limit performance is critical to advancing BTF cells. We show that recombination at the back interface has limited device performance of fabricated BTF devices. Improved BTF performance will require decreasing recombination at the back interface, through passivation or by reducing downward band-bending at this interface. Increasing carrier lifetimes improves performance, but increasing hole density has little effect.

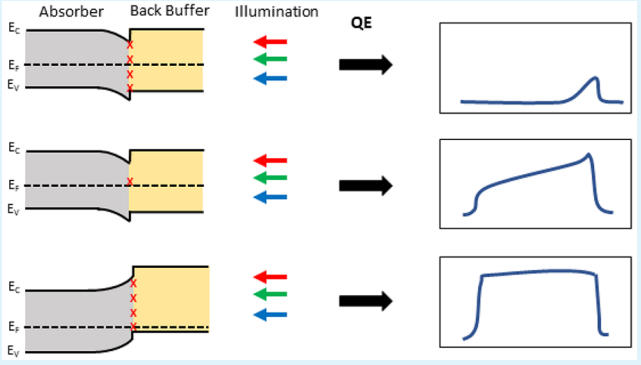

KEYWORDS: *bifacial, thin film, CdTe, numerical modeling, IFLO, recombination, solar cells*

With single junction photovoltaic (PV) device efficiencies exceeding 25%,[1] new solar cell architectures will be needed to allow the power production per unit area to be increased. One of the most promising and potentially inexpensive methods to increase the power production per unit area of single junction devices is to use a bifacial configuration. This configuration allows for photons to enter the absorber through both sides of the device, allowing reflected and scattered light incident on the back surface to boost the power output. Early measurements showed that bifacial devices could produce 50% more power under certain conditions.[2] More recent studies show that mounting bifacial modules on high albedo backgrounds can result in an energy yield increase of ∼20−30%.[3,4] On the basis of these benefits, the International Technology Roadmap for Photovoltaics estimates that bifacial devices will account for ∼40% of the PV market by 2028.[5]

Due to the potential for a significant increase in energy yield, there has been substantial interest in developing bifacial devices. Most of this work has been on high efficiency crystalline Si devices, which are now deployed in the market,[6] but research into bifacial thin film (BTF) PV has begun.[7−10] In Si PV devices, a long bulk carrier lifetime (hundreds of microseconds to milliseconds)[11,12] and long diffusion length coupled with low surface recombination velocities (SRVs; ∼10 cm s^{-1})[12] means that carriers can reach the carrier selective contacts before recombining, regardless of the direction of the incoming light. When paired with the development of transparent back contacts, bifacial Si devices efficiencies of 19.5−22% and 17−19% have been achieved when illuminated through the front and rear of the device, respectively.[13] These values result in a bifaciality, defined as the ratio of efficiency illuminated through the back to efficiency illuminated through the front, of 85%.

Progress in improving the bifacial performance of polycrystalline thin film PV has been limited by relatively short measured minority carrier lifetimes on the order of 1 ns[14] and high back surface recombination velocities on the order of ∼10^5 cm s^{-1}.[15] Under these conditions, the device efficiency is low (5.0% for CdTe[9] and 6.0% for CIGS[8]) when illuminated through the back side (η_{Back}) even when the front-illuminated efficiency (η_{Front}) is high. Recent improvements in the carrier lifetime with Se incorporated into CdTe[16,17] and companion reports of diffusion lengths much greater than the typical device thickness[17] suggest that it should be possible to fabricate high performance BTF CdTe devices. To date, however, understanding of the deficiencies of bifacial thin film devices has been limited to generalizations about absorber thickness[7,10] or analysis of the PV parameters.[9] Recent modeling indicates that a highly doped back buffer layer[18] or reduction in back surface recombination velocity (BSRV)[8] can lead to improved device performance for bifacial CIGS, but there is still a lack of general understanding.

Received: April 16, 2020
Accepted: June 9, 2020
Published: June 9, 2020

https://dx.doi.org/10.1021/acsaem.0c00851
ACS Appl. Energy Mater. 2020, 3, 6072−6078

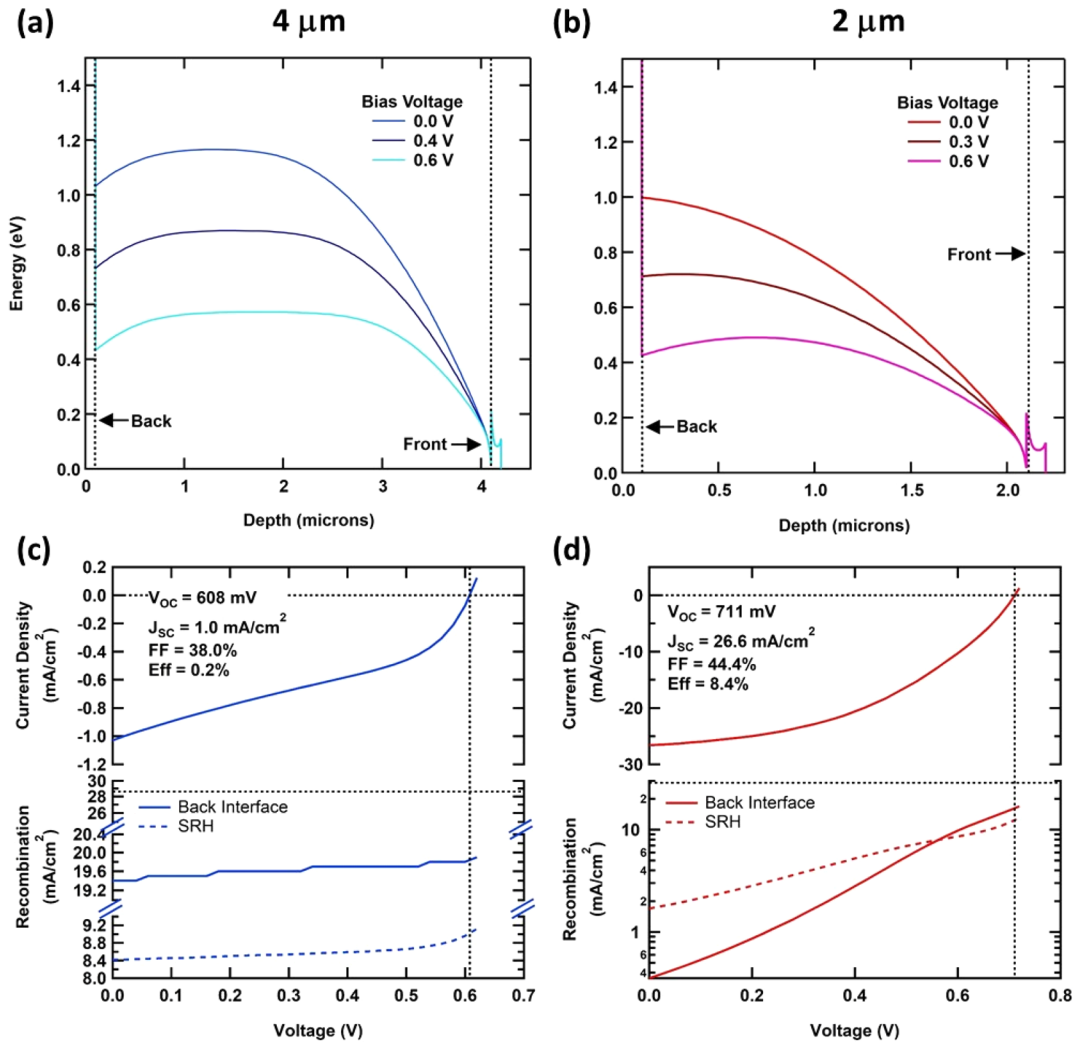

Figure 1. (a, b) Conduction band portion of the band diagrams for 4 and 2 μm absorber thickness devices, respectively, at various bias voltages. Note that the back of the device is located on the left. (c, d) Corresponding current (J) and recombination current densities (J_r) as a function of bias voltage.

Here, we use numerical simulations to determine critical factors for device designs that will allow the simultaneous optimization of both front side and back side illumination performance. We evaluate the relative importance of carrier lifetime, absorber dopant density, and absorber thickness and consider approaches to reducing the recombination at the back interface through either chemical passivation or the production of a back surface field. Our findings can be used to guide real-world efforts to push the efficiency of back side illuminated thin film PV devices closer to that of monofacial devices, thereby increasing bifacial performance and increasing the overall power output.

Simulations were carried out using SCAPS-1D software version 3.3.05.[19] Following previous work,[20] modeled devices consisted of a 300 nm n-type transparent front contact, a 100 nm $Zn_xMg_{1-x}O$ (ZMO) emitter layer, a CdTe layer of variable thickness, a 100 nm back side buffer, and a transparent back electrode. The ZMO composition was chosen to produce a bandgap of 3.7 eV with a conduction band that was 0.2 eV higher than the conduction band of CdTe (conduction band offset of +0.2 eV). This configuration has been shown to produce very low front surface recombination currents that can be neglected for all conditions examined here.[21,22] The back buffer layer was chosen with a valence band 0.2 eV higher in energy than the valence band of CdTe (valence band offset of −0.2 eV) and a bandgap of 3.3 eV to be a transparent contact. Typically, in BTF devices, an n-type transparent conducting oxide (TCO) is deposited at the back of the device.[7−10] However, implementation of a traditional n-type TCO on both sides of the device is not permitted in the SCAPS software, so the bands between the buffer and transparent back contact were fixed to be flat. While the effects of the n-type TCO at the back of a p-type absorber and buffer on the band diagram are not well-understood in BTF devices, we expect this to induce downward band-bending in the buffer at the buffer/TCO interface. We have recently showed that if a low barrier for hole flow can be maintained, this band-bending does not alter the device performance.[20] Recent measurements suggest that this may be the case.[23] The key material parameters, except where noted, were obtained from the literature and are presented in the SI. Following earlier work,[22] we chose Gaussian type midgap defect states with electron and hole carrier lifetimes equal to each other with specific values noted in the text. The back surface recombination velocity (BSRV) was held at 10^4 cm s^{-1} (an order of magnitude lower than typical values). Other material parameters for the buffer layer were set to those

https://dx.doi.org/10.1021/acsaem.0c00851
ACS Appl. Energy Mater. 2020, 3, 6072−6078

Table 1. Back-Illuminated PV Parameters for Two Absorber Thicknesses as a Function of Back Surface Recombination Velocity (BSRV)[a]

	4 μm					2 μm				
BSRV, cm s^{-1}	V_{OC}, mmV	J_{SC}, mA cm^{-2}	FF %	eff %	bifac	V_{OC}, mV	J_{SC}, mA cm^{-2}	FF %	eff %	bifac
10^4	751	2.3	44.3	0.8	0.04	755	28.2	51.5	11.0	0.6
10^3	813	11.1	49.2	4.4	0.22	820	28.6	68.6	16.1	0.84
10^2	893	23.2	66.9	13.9	0.69	905	28.6	75.2	19.5	0.98
10^1	924	25.8	71.9	17.2	0.85	943	28.6	75.6	20.4	1
10^0	929	26.1	72.5	17.6	0.87	949	28.6	75.6	20.5	1

[a]The bifaciality (bifac) is defined as efficiency illuminated through the back divided by efficiency illuminated through the front.

used for the CdTe. For back side illumination, the absorption in the buffer layer was set to zero to ensure computational convergence.

We first investigated the performance limitations of the best reported BTF devices with back side illumination by considering the band diagrams and the controlling recombination currents.[9,10] To understand previously fabricated devices, we used values that are representative of the materials properties of those devices. The initial carrier lifetimes were set to 1 ns.[24] The CdTe hole density was set to 2×10^{14} cm^{-3}, and the back buffer hole density was 2×10^{14} cm^{-3}, which corresponds to an initial Fermi level offset (IFLO) of −0.2 eV.[20] Note that because of the deep valence band position of CdTe, it is difficult to make an Ohmic contact. We use IFLO to characterize this contact. A negative IFLO results in downward band-bending and the formation of a Schottky junction. The typical back contact for CdTe devices results in a negative IFLO. A positive IFLO results in upward band-bending and would indicate an Ohmic contact. In addition, higher positive IFLO indicates a more carrier selective contact. The −0.2 eV IFLO value used here produces band-bending at the rear contact which is similar to that found with a Te back contact.[25]

Panels a and b of Figure 1 show the conduction band portion of the simulated band diagrams at three different biases for devices with absorber thicknesses of 4 and 2 μm, respectively, while illuminated through the back side of the device. Note that these thicknesses are representative of the experimental bifacial CdTe absorber thicknesses.[7,9,10] Panels c and d show the corresponding current density and recombination current density versus voltage (J−V and J_r−V) plots, respectively. The behavior of the devices can be understood by considering how the band-bending at the front (emitter/absorber) and back (absorber/back buffer) junctions (FJ and BJ, respectively) interact to form the overall band diagrams, and how the band-bending and recombination currents change with bias.

In the 4 μm device, the FJ depletion width extends from ∼2 to 4 μm (2 μm total) in the CdTe layer at zero bias. At a 0.3 or 0.6 V bias, the FJ depletion width decreases and extends from 2.5 or 3 μm, respectively, to 4 μm. The downward bending depletion width at the BJ, on the other hand, extends from 0 to 1 μm and is nearly independent of the bias voltage. With back side illumination, the penetration depth of the ultraviolet and visible wavelength light is short, and a large fraction of the carrier generation with AM1.5 irradiance occurs within ∼1 μm of the back surface. With bias-independent band-bending near the BJ, the carriers are swept in the wrong direction, and the interface recombination current (J_{INT}) is high, leading to a low J_{SC}. As the bias voltage increases, the band-bending at the FJ decreases. This leads to a decrease in the number of carriers that are collected at the FJ. Furthermore, the flattening of the bands with increasing bias causes the Shockley−Reed−Hall (SRH) recombination current density (J_{SRH}) to turn-on smoothly over a wide voltage range. This smooth, as opposed to abrupt, increase in J_{SRH} with bias results in a low fill factor (FF). In this case, the J_{INT} remains higher than J_{SRH} at all biases.

For the 2 μm device, the FJ and BJ are close enough that they interact to significantly affect the overall band diagram. Interestingly, at zero bias, there is no BJ depletion region. This gives rise to a much higher J_{SC}. As with the 4 μm absorber case, increasing the bias reduces the band-bending at the FJ. This allows a downward bending depletion region at the BJ to begin to emerge. This results in a bias-dependent increase in the back surface J_{INT} and, thus, a low FF. Interestingly, J_{INT} is lower than J_{SRH} until ∼550 mV, but ∼1.5 times larger by V_{OC}.

To improve the device performance during back side illumination, it is clear that the back interface recombination needs to be reduced. Productive strategies could be similar to those employed for improving the front side performance of CdTe devices[16] and other thin film PV materials,[26,27] which typically involve either chemical passivation of defects[28] or modification of the surface electric field and the related band-bending.[11]

Considering chemical passivation of the back interface first, we examined the effect of decreasing the back surface recombination velocity (BSRV) from 10^4 to 10^0 cm s^{-1} for $p_{CdTe} = 2 \times 10^{14}$ cm^{-3}. Again, we considered both 4 and 2 μm thick absorber layers, but in this case the carrier lifetimes were increased to 32 ns to be closer to recently measured values.[14,16] Note that the increased lifetime accounts for suppression of bulk defect states as well as improved passivation of the grain boundaries in the polycrystalline absorber layer. Table 1 shows the resultant simulated PV parameters and the bifaciality metric (η_{Back}/η_{Front}). As expected, reducing the BSRV results in lower recombination at this interface, leading to increases in both J_{SC} and FF in the 4 μm device, and an increase in the FF in the 2 μm device. It is surprising, however, that the bifaciality of the 4 μm device does not reach 1. This is due to the fact that the downward bending depletion region exists at the BJ for all biases. Thus, carriers generated near the BJ cannot reach the front of the device before recombining through the SRH mechanism, even at zero bias. For a 2 μm device, on the other hand, there is no depletion region at the BJ at zero bias. As a result, J_{INT} is low, and J_{SC} is high for all values of BSRV. In the thin absorber case, reducing the BSRV leads to improved FF. Interestingly, the bifaciality approaches 1 as the BSRV is reduced to 10^2 cm s^{-1}. In both cases, reducing the BSRV to values lower than 10^1 cm s^{-1} does not further improve the device performance because J_{INT} is already an order of magnitude lower that J_{SRH} (SI).

https://dx.doi.org/10.1021/acsaem.0c00851
ACS Appl. Energy Mater. 2020, 3, 6072−6078

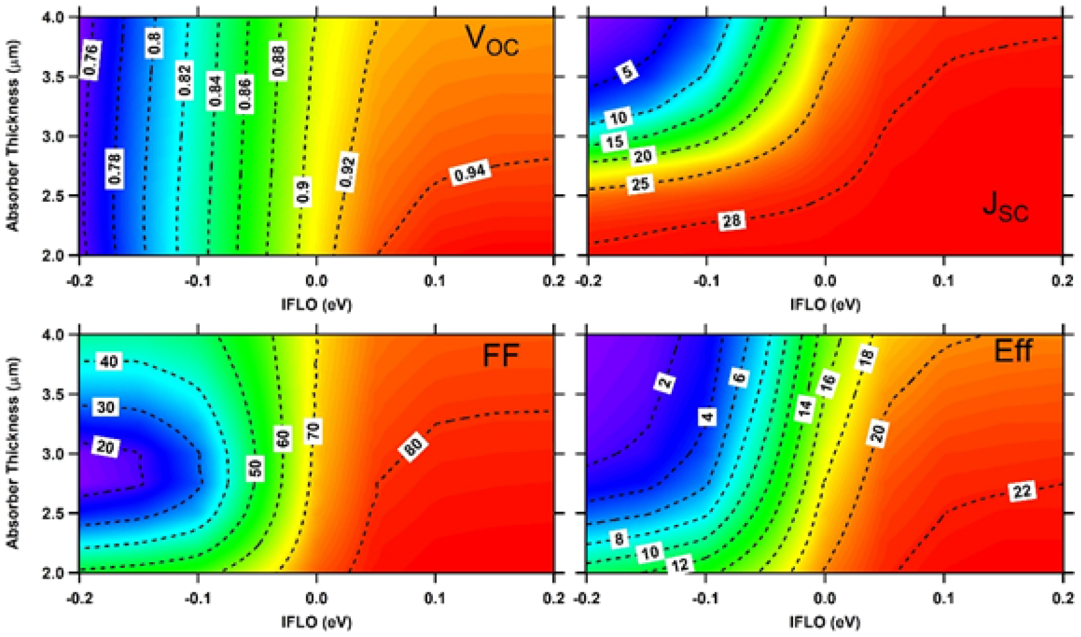

Figure 2. Contour plots of the back-illuminated PV parameters for devices of varying thickness as a function of initial Fermi level offset (IFLO). The carrier lifetime was maintained at 32 ns; the BSRV was 1×10^4 cm s^{-1}, and p_{CdTe} was 2×10^{14} cm^{-3}.

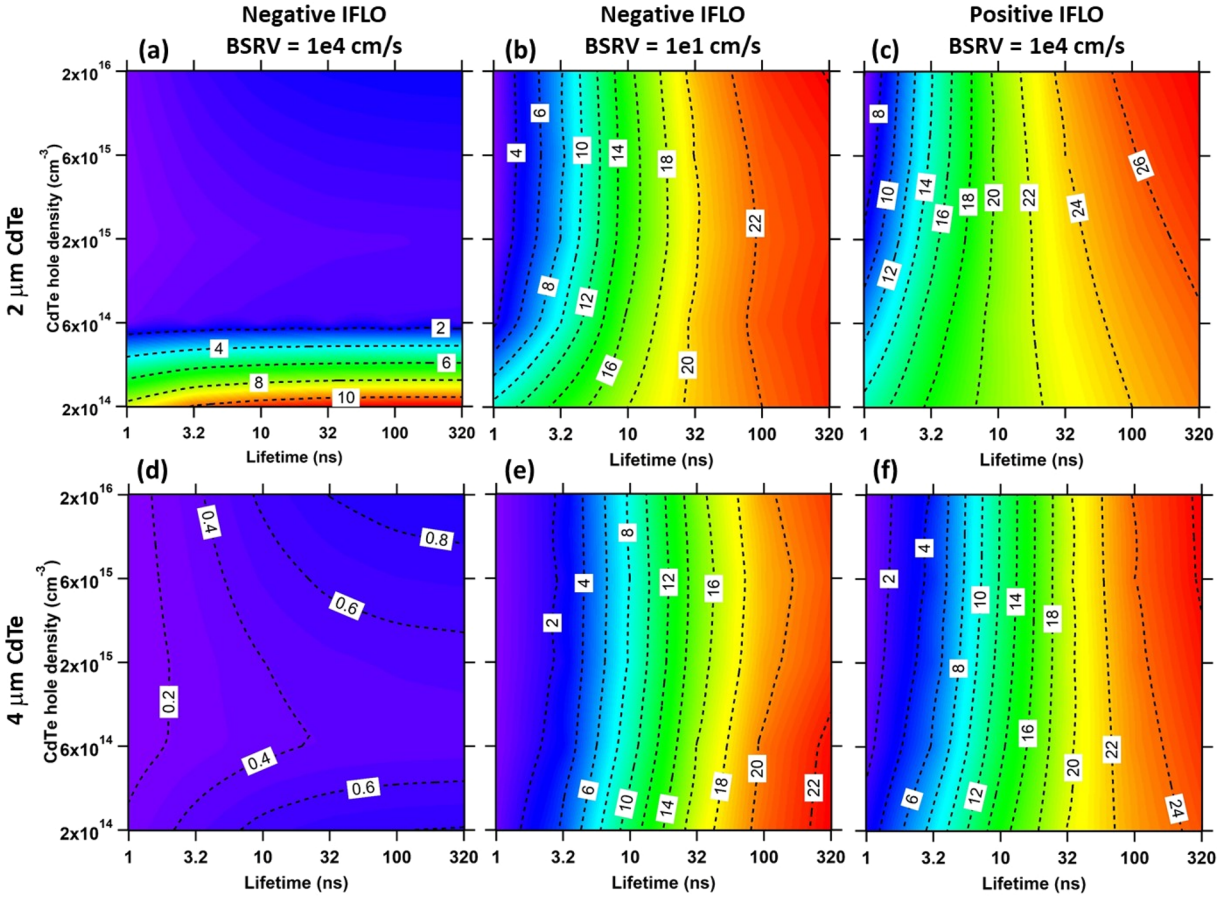

Figure 3. Contour plots of the back-illuminated efficiency as a function of absorber hole density and carrier lifetime for absorber thicknesses, (a−c) 2 μm and (d−f) 4 μm, and varying back interface conditions: (a, d) negative IFLO, BSRV = 1×10^4 cm s^{-1}; (b, e) negative IFLO, BSRV = 1×10^1 cm s^{-1}; and (c, f) positive IFLO, BSRV = 1×10^4 cm s^{-1}.

Band-bending can also be modified by locating fixed charge at the back buffer layer[11] or, more generally, by changing the alignment of the noninteracting initial Fermi level offset (IFLO) between the absorber and buffer.[20] (See SI for how fixed charges relate to IFLO.) Figure 2 shows contour plots of the back-illuminated PV parameters as a function of the IFLO

https://dx.doi.org/10.1021/acsaem.0c00851
ACS Appl. Energy Mater. 2020, 3, 6072−6078

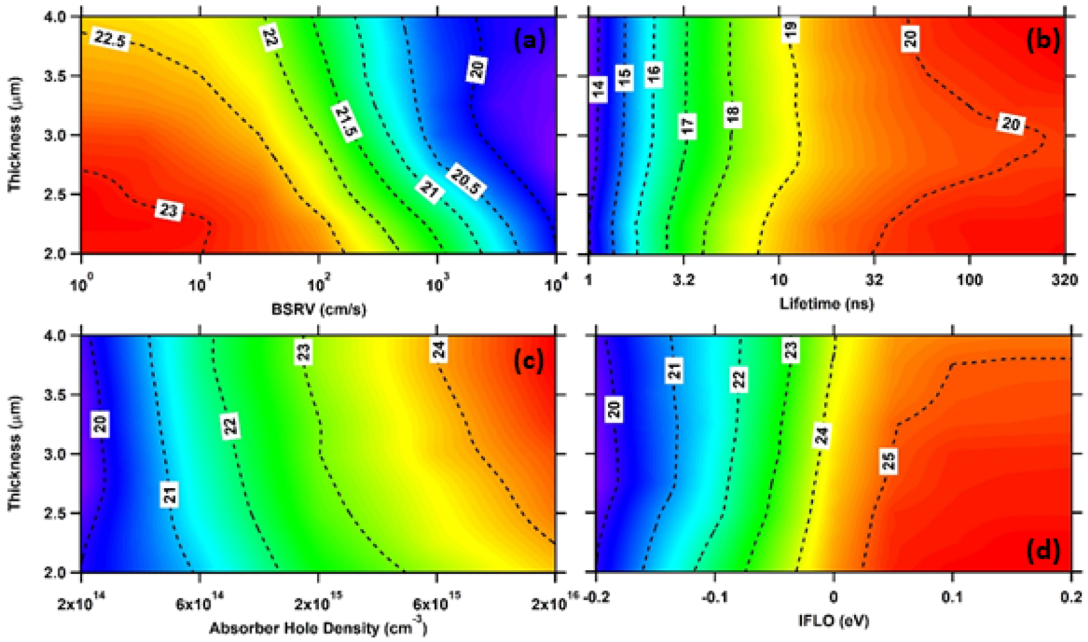

Figure 4. Contour plots of bifacial efficiency as a function of thickness and (a) BSRV, (b) lifetime, (c) CdTe hole density, and (d) IFLO. When not varied, the following conditions applied: the BSRV was set to 10^4 cm/s; the carrier lifetime was set to 32 ns; the CdTe hole density was set to 2×10^{14} cm^{-3}; and the IFLO was set to −0.2 eV.

and the absorber thickness. The data for devices illuminated through the front interface and the ratio of front/back-illumination performance are shown in the SI. The J_{SC} decreases with increasing thickness for negative values of the IFLO because the BJ controls the performance. On the other hand, when the IFLO is positive, there is upward band-bending at the BJ and J_{SC} is not strongly affected by thickness. In general, thinner CdTe devices tend to produce higher η_{Back} for all IFLOs. This is in contrast to devices illuminated through the front side when the IFLO is negative. When this is the case, the BJ and FJ interact (see Figure 1) which reduces the overall band-bending in the device and results in lower V_{OC} and η_{Front}. As the absorber thickness increases, the interaction between the FJ and BJ decreases and becomes negligible ∼3.5 μm. However, devices with proper band-bending (IFLO > 0.05 eV) perform well for both thicknesses, and the bifaciality approaches unity.

Reducing the recombination at the back of the device by passivation or by creating preferred band-bending is critical for high efficiency back side illuminated devices, but other parameters are important as well.[29] Figure 3 shows contour plots of the efficiency as a function of CdTe hole density and carrier lifetime for 2 and 4 μm devices illuminated through the back side for various back interface conditions. The corresponding PV parameters are shown in the SI. When there is a bad BJ (negative IFLO and BSRV = 1×10^4 cm-s^{-1}; Figure 3a,d), the devices are back interface limited. For the 2 μm device, the efficiencies are higher at the lower hole density values because the FJ depletion region extends to the back of the device under these conditions and the current collection can be effective. However, when there are distinct FJ and BJ depletion regions, carriers recombine at the back interface resulting in poor current collection, and the efficiency is low. This condition is found when the hole density is high in the 2 μm devices and occurs for all values of hole density in the 4 μm devices.

When the BSRV is low (10 cm s^{-1}; Figure 3b,e) or the bands are bent upward at the back interface (positive IFLO; Figure 3c,f), the back side performance is no longer limited by the back interface. Increasing the lifetime leads to a higher bias onset for SRH recombination and higher efficiency, while increasing the hole density has little effect on the back side performance in these cases. Interestingly, when illuminated through the back side, the 2 μm devices have higher efficiency than the 4 μm devices at a given doping level and lifetime, but the opposite is true when devices are illuminated through the front side. This suggests that there may be an optimum absorber thickness for a BTF device.

To provide some insight, we considered a device operating on a background surface with an albedo of 15%, and summed the relative front side and back side illumination efficiencies to calculate a bifacial efficiency ($\eta_{Bi} = \eta_{Front}$(at 1 sun) + η_{Back}(at 15% of 1 sun)). Note that the back side illumination of bifacial devices is significantly lower than the 1 sun value used for all the simulations above. Even at the low intensity, the back side illuminated *JV* curves generated here follow the familiar pattern for reduced intensity: linear reduction in J_{SC} and logarithmic reduction in V_{OC}. Figure 4 shows the bifacial efficiency as a function of absorber thickness and BSRV, lifetime, hole density, and IFLO. Note that when these parameters were not specifically varied, they were fixed to 10^4 cm/s, 32 ns, 2×10^{14} cm^{-3}, and −0.2 eV, respectively, indicating a poor back interface.

Figure 4 illustrates three main points. First, when the back interface is improved through reduced BSRV (Figure 4a) or increased IFLO (Figure 4d), a thinner absorber produces a higher efficiency BTF device. Second, for any given carrier lifetime greater than ∼20 ns (Figure 4b), the bifacial efficiency is high for the 2 μm absorber, decreases until the absorber thickness is ∼3 μm, and then increases again, with the thinnest devices having the highest bifacial efficiency. Third, when the absorber hole density is high (Figure 4c), the BTF device performance is dictated by the front-illuminated performance.

https://dx.doi.org/10.1021/acsaem.0c00851
ACS Appl. Energy Mater. 2020, 3, 6072−6078

These results indicate that when the recombination at the BJ is low, thinner BTF devices can perform better than thick devices.

CONCLUSIONS

Using numerical simulations, we showed that BTF devices fabricated to date have been limited by recombination at the back interface. Improvement in the bifacial performance of thin film devices will require improving the back interface through either passivation and/or by reducing the downward band-bending at this interface. We also showed that back side illuminated devices depend strongly on doping density when the back interface is bad but depend strongly on the carrier lifetimes and weakly on absorber hole density when the back interface is good. Finally, we showed that thinner BTF devices may perform better than thicker when the absorber doping density is low or the back interface recombination can be reduced through passivation or decreases downward band-bending at the current carrier lifetimes.

ASSOCIATED CONTENT

Supporting Information

The Supporting Information is available free of charge at https://pubs.acs.org/doi/10.1021/acsaem.0c00851.

SCAPS parameters; IFLO sign convention; QE of existing devices; effects of BSRV; converting fixed charges to IFLO; and effects of IFLO, absorber hole density, and carrier lifetime on other PV parameters (PDF)

AUTHOR INFORMATION

Corresponding Author

Adam B. Phillips − *Wright Center for Photovoltaics Innovation and Commercialization, Department of Physics and Astronomy, University of Toledo, Toledo, Ohio 43606, United States;* orcid.org/0000-0002-2675-5052; Email: Adam.Phillips@UToledo.edu

Authors

Kamala Khanal Subedi − *Wright Center for Photovoltaics Innovation and Commercialization, Department of Physics and Astronomy, University of Toledo, Toledo, Ohio 43606, United States*

Geethika K. Liyanage − *Wright Center for Photovoltaics Innovation and Commercialization, Department of Physics and Astronomy, University of Toledo, Toledo, Ohio 43606, United States;* orcid.org/0000-0003-4000-0729

Fadhil K. Alfadhili − *Wright Center for Photovoltaics Innovation and Commercialization, Department of Physics and Astronomy, University of Toledo, Toledo, Ohio 43606, United States*

Randy J. Ellingson − *Wright Center for Photovoltaics Innovation and Commercialization, Department of Physics and Astronomy, University of Toledo, Toledo, Ohio 43606, United States;* orcid.org/0000-0001-9520-6586

Michael J. Heben − *Wright Center for Photovoltaics Innovation and Commercialization, Department of Physics and Astronomy, University of Toledo, Toledo, Ohio 43606, United States;* orcid.org/0000-0002-3788-3471

Complete contact information is available at: https://pubs.acs.org/10.1021/acsaem.0c00851

Notes

The authors declare no competing financial interest.

The U.S. Government is authorized to reproduce and distribute reprints for Governmental purposes notwithstanding any copyright notation thereon. The views and conclusions contained herein are those of the authors and should not be interpreted as necessarily representing the official policies or endorsements, either expressed or implied, of Air Force Research Laboratory or the U.S. Government.

ACKNOWLEDGMENTS

This material is based on research sponsored by Air Force Research Laboratory under agreement FA9453-18-2-0037 and by the U.S. DOE's Office of Energy Efficiency and Renewable Energy (EERE) under Solar Energy Technologies Office (SETO) Agreement DE-EE0008974.

REFERENCES

(1) Green, M. A.; Dunlop, E. D.; Levi, D. H.; Hohl-Ebinger, J.; Yoshita, M.; Ho-Baillie, A. W. Y. Solar cell efficiency tables (version 54). *Prog. Photovoltaics* **2019**, *27* (7), 565−575.

(2) Cuevas, A.; Luque, A.; Eguren, J.; del Alamo, J. 50% more output power from an albedo-collecting flat panel using bifacial solar cells. *Sol. Energy* **1982**, *29* (5), 419−420.

(3) Yusufoglu, U. A.; Pletzer, T. M.; Koduvelikulathu, L. J.; Comparotto, C.; Kopecek, R.; Kurz, H. Analysis of the annual performance of bifacial modules and optimization methods. *Journal of Photovoltaics* **2015**, *5* (1), 320−328.

(4) Sun, X.; Khan, M. R.; Deline, C.; Alam, M. A. Optimization and performance of bifacial solar modules: A global perspective. *Appl. Energy* **2018**, *212*, 1601−1610.

(5) Fischer, M. In *ITRPV 9th Edition 2018 Report Release and Key Findings*; PV CellTech conference, 2018.

(6) Liang, T. S.; Pravettoni, M.; Deline, C.; Stein, J. S.; Kopecek, R.; Singh, J. P.; Luo, W.; Wang, Y.; Aberle, A. G.; Khoo, Y. S. A review of crystalline silicon bifacial photovoltaic performance characterisation and simulation. *Energy Environ. Sci.* **2019**, *12* (1), 116−148.

(7) Romeo, A.; Khrypunov, G.; Galassini, S.; Zogg, H.; Tiwari, A. Bifacial configurations for CdTe solar cells. *Sol. Energy Mater. Sol. Cells* **2007**, *91* (15−16), 1388−1391.

(8) Keller, J.; Chen, W. C.; Riekehr, L.; Kubart, T.; Törndahl, T.; Edoff, M. Bifacial Cu(In, Ga)Se_2 solar cells using hydrogen-doped In_2O_3 films as a transparent back contact. *Prog. Photovoltaics* **2018**, *26* (10), 846−858.

(9) Marsillac, S.; Parikh, V.; Compaan, A. Ultra-thin bifacial CdTe solar cell. *Sol. Energy Mater. Sol. Cells* **2007**, *91* (15−16), 1398−1402.

(10) Khanal, R. R.; Phillips, A. B.; Song, Z.; Xie, Y.; Mahabaduge, H. P.; Dorogi, M. D.; Zafar, S.; Faykosh, G. T.; Heben, M. J. Substrate configuration, bifacial CdTe solar cells grown directly on transparent single wall carbon nanotube back contacts. *Sol. Energy Mater. Sol. Cells* **2016**, *157*, 35−41.

(11) Agostinelli, G.; Delabie, A.; Vitanov, P.; Alexieva, Z.; Dekkers, H.; De Wolf, S.; Beaucarne, G. Very low surface recombination velocities on p-type silicon wafers passivated with a dielectric with fixed negative charge. *Sol. Energy Mater. Sol. Cells* **2006**, *90* (18−19), 3438−3443.

(12) Wan, Y.; McIntosh, K. R.; Thomson, A. F.; Cuevas, A. Low surface recombination velocity by low-absorption silicon nitride on c-Si. *2012 IEEE 38th Photovoltaic Specialists Conference (PVSC)* **2012**, 1−7.

(13) Dullweber, T.; Schulte-Huxel, H.; Blankemeyer, S.; Hannebauer, H.; Schimanke, S.; Baumann, U.; Witteck, R.; Peibst, R.; Köntges, M.; Brendel, R.; Yao, Y. Present status and future perspectives of bifacial PERC+ solar cells and modules. *Jpn. J. Appl. Phys.* **2018**, *57* (8S3), 08RA01.

https://dx.doi.org/10.1021/acsaem.0c00851
ACS Appl. Energy Mater. 2020, 3, 6072−6078

(14) Gloeckler, M.; Sankin, I.; Zhao, Z. CdTe solar cells at the threshold to 20% efficiency. *IEEE Journal of Photovoltaics* **2013**, *3* (4), 1389−1393.
(15) Kuciauskas, D.; Kanevce, A.; Burst, J. M.; Duenow, J. N.; Dhere, R.; Albin, D. S.; Levi, D. H.; Ahrenkiel, R. K. Minority carrier lifetime analysis in the bulk of thin-film absorbers using subbandgap (two-photon) excitation. *Journal of Photovoltaics* **2013**, *3* (4), 1319−1324.
(16) Kephart, J. M.; Kindvall, A.; Williams, D.; Kuciauskas, D.; Dippo, P.; Munshi, A.; Sampath, W. Sputter-deposited oxides for interface passivation of CdTe photovoltaics. *Journal of Photovoltaics* **2018**, *8* (2), 587−593.
(17) Kuciauskas, D.; Moseley, J.; Ščajev, P.; Albin, D. Radiative Efficiency and Charge-Carrier Lifetimes and Diffusion Length in Polycrystalline CdSeTe Heterostructures. *Phys. Status Solidi RRL* **2020**, *14*, 1900606.
(18) Mouhoub, A.; Bouloufa, A.; Djessas, K.; Messous, A. Analytical modeling and optimization of original bifacial solar cells based on Cu (In, Ga) Se2 thin films absorbers. *Superlattices Microstruct.* **2018**, *122*, 434−443.
(19) Burgelman, M.; Nollet, P.; Degrave, S. Modelling polycrystalline semiconductor solar cells. *Thin Solid Films* **2000**, *361*, 527−532.
(20) Liyanage, G. K.; Phillips, A. B.; Alfadhili, F. K.; Ellingson, R. J.; Heben, M. J. The role of back buffer layers and absorber properties for> 25% efficient CdTe solar cells. *ACS Applied Energy Materials* **2019**, *2* (8), 5419−5426.
(21) Ablekim, T.; Colegrove, E.; Metzger, W. K. Interface Engineering for 25% CdTe Solar Cells. *ACS Applied Energy Materials* **2018**, *1* (10), 5135−5139.
(22) Song, T.; Kanevce, A.; Sites, J. R. Emitter/absorber interface of CdTe solar cells. *J. Appl. Phys.* **2016**, *119* (23), 233104.
(23) Watthage, S. C.; Phillips, A. B.; Liyanage, G. K.; Song, Z.; Gibbs, J. M.; Alfadhili, F. K.; Alkhayat, R. B.; Ahangharnejhad, R. H.; Almutawah, Z. S.; Bhandari, K. P.; et al. Selective Cd Removal From CdTe for High-Efficiency Te Back-Contact Formation. *IEEE J. Photovoltaics* **2018**, *8* (4), 1125−1131.
(24) Paudel, N. R.; Young, M.; Roland, P. J.; Ellingson, R. J.; Yan, Y.; Compaan, A. D. Post-deposition processing options for high-efficiency sputtered CdS/CdTe solar cells. *J. Appl. Phys.* **2014**, *115* (6), 064502.
(25) Niles, D. W.; Li, X.; Sheldon, P.; Höchst, H. A photoemission determination of the band diagram of the Te/CdTe interface. *J. Appl. Phys.* **1995**, *77* (9), 4489−4493.
(26) Guarnera, S.; Abate, A.; Zhang, W.; Foster, J. M.; Richardson, G.; Petrozza, A.; Snaith, H. J. Improving the long-term stability of perovskite solar cells with a porous Al_2O_3 buffer layer. *J. Phys. Chem. Lett.* **2015**, *6* (3), 432−437.
(27) Vermang, B.; Fjällström, V.; Gao, X.; Edoff, M. Improved Rear Surface Passivation of Cu (In, Ga)Se_2 Solar Cells: A Combination of an Al_2O_3 Rear Surface Passivation Layer and Nanosized Local Rear Point Contacts. *Journal of Photovoltaics* **2014**, *4* (1), 486−492.
(28) Dingemans, G.; Beyer, W.; Van de Sanden, M.; Kessels, W. Hydrogen induced passivation of Si interfaces by Al_2O_3 films and SiO2/Al2O3 stacks. *Appl. Phys. Lett.* **2010**, *97* (15), 152106.
(29) Kanevce, A.; Reese, M. O.; Barnes, T.; Jensen, S.; Metzger, W. The roles of carrier concentration and interface, bulk, and grain-boundary recombination for 25% efficient CdTe solar cells. *J. Appl. Phys.* **2017**, *121* (21), 214506.

https://dx.doi.org/10.1021/acsaem.0c00851
ACS Appl. Energy Mater. 2020, 3, 6072−6078